

5-7-2015

Magnetoresistance Characteristics in Individual Fe_3O_4 Single Crystal Nanowire

K. M. Reddy
Boise State University

Nitin P. Padture
Brown University

Alex Punnoose
Boise State University

Charles Hanna
Boise State University

Magnetoresistance characteristics in individual Fe₃O₄ single crystal nanowire

K. M. Reddy,^{1,a)} Nitin P. Padture,² Alex Punnoose,¹ and Charles Hanna¹

¹Department of Physics, Boise State University, Boise, Idaho 83725, USA

²School of Engineering, Brown University, Providence, Rhode Island 02912, USA

(Presented 5 November 2014; received 19 September 2014; accepted 2 November 2014; published online 11 March 2015)

We report on the magnetoresistance (MR) and electron transport measurements observed on a single crystal magnetite nanowire prepared using a hydrothermal synthesis method. High-resolution electron microscopy revealed the single crystal magnetite nanowires with 80–120 nm thickness and up to 8 μm in length. Magnetic measurements showed the typical Verwey transition around 120 K with a 100 Oe room temperature coercivity and 45 emu/g saturation magnetization, which are comparable to bulk magnetite. Electrical resistance measurements in 5–300 K temperature range were performed by scanning gate voltage and varying applied magnetic field. Electrical resistivity of the nanowire was found to be around $5 \times 10^{-4} \Omega \text{ m}$, slightly higher than the bulk and has activation energy of 0.07 eV. A negative MR of about 0.7% is observed for as-synthesized nanowires at 0.3 T applied field. MR scaled with increasing applied magnetic field representing the field-induced alignment of magnetic domain. These results are attributed to the spin-polarized electron transport across the antiphase boundaries, which implicate promising applications for nanowires in magnetoelectronics. © 2015 AIP Publishing LLC. [<http://dx.doi.org/10.1063/1.4914535>]

Being part of the Half-metal family, magnetite (Fe₃O₄) has been the subject of research focus recently due to its potential applications in magnetoelectronics.^{1–3} Magnetite is predicted to display a 100% spin polarization at the Fermi level, with majority spin electrons exhibiting insulating or semiconducting behavior, while the minority spins showing metallic behavior.² Unusually high Curie temperature (858 K) of Fe₃O₄ facilitates device integration at room temperature for magneto-electronic applications. Bulk and polycrystalline magnetite was found to have more than 10% magnetoresistance (MR),^{4,5} which is still far below the theoretical prediction. The observed MR is attributed to spin polarized electron injection through tunnel barriers, grain boundaries, and interparticle contacts.^{6,7} Defects, reconstruction at the surface and interfaces, strain effects, and off-stoichiometry reduce the spin-polarized current.⁸ Material microstructure, coercivity, grain size, grain boundary structure, and crystallite orientations define the intrinsic properties of magnetite for spintronics applications.² Unprecedented technology advancements in miniaturizing the device integration are driving the research at nanoscale. MR and electron transport studies on magnetite were largely focused on thin films, bulk, nanocrystal assemblies, and compact powder forms.^{2,4,9–11} Shape anisotropy and the low-dimensionality of nanostructures play critical role in determining the spin transport properties. However, there are very few reports in the literature focusing magnetotransport on the magnetite nanostructures.

One-dimensional (1D) nanostructures have unique electron transport properties compared to bulk and have shown

potential applications in nanodevice electronics. Several attempts were made by researchers to understand the magnetic and electronic properties of 1D Fe₃O₄ nanowires. Liu *et al.*¹² studied the magnetotransport in individual single crystal magnetite nanotube and observed a negative 1% MR at 77 K and 0.7 T applied field. Magnetic microstructure of 1D Fe₃O₄ nanowires was studied by mapping the magnetic flux by electron holography¹³ suggesting the possibility of regulating spin current, apart from understanding the magnetic behavior using SQUID magnetometer. Epitaxially grown MgO/Fe₃O₄ core shell nanostructures were found to have 1.2% MR at room temperature under 1.8 T applied field, which is credited to the tunneling of spin-polarized electrons across the antiphase boundaries.¹⁴ Terrier *et al.* measured the transport properties of several polycrystalline nanowires and reported 8.5% MR at room temperature and did not observe any anisotropy.¹⁵ The magneto-electron transport properties of an individual single crystalline Fe₃O₄ nanowire are still inconsistent. All the aforementioned studies attribute the MR response to tunneling of spin-polarized electrons across grain boundaries or interparticle contact. However, it would be interesting to study the MR using a single crystalline nanowire eliminating the interparticle contacts and grain boundaries. To this effect, Liao *et al.* have observed an anomalous 7.5% positive MR on individual magnetite nanowire, and the device demonstrated a spin-filter effect, prepared through hydrothermal method.¹⁶ But, unusual positive MR¹⁶ observation in single crystal nanowire is contradicting the negative MR observed with epitaxial thin films, bulk and polycrystalline Fe₃O₄.^{2,4,14,17,18} In this report, we discuss the magneto-electron transport properties from a single crystalline magnetite nanowire that exhibits negative MR.

^{a)}Author to whom correspondence should be addressed. Electronic mail: mrkongara@boisestate.edu.

Single crystal Fe_3O_4 nanowires were prepared by a simple hydrothermal method. In a typical process, FeSO_4 , $\text{Na}_2\text{S}_2\text{O}_3$, and NaOH are mixed in 2:1:25 molar ratio and ground thoroughly. The mixture is then transferred to a Teflon lined autoclave containing polyethylene glycol (molecular weight—4000) in water (3:1). The autoclave is subjected to heat treatment at 160°C for 24 h and cooled to room temperature naturally. The contents are washed with water and ethanol to remove the polymer residue and vacuum dried. The samples were probed with X-ray diffractometer (Sintag XDS 2000), scanning electron microscopy (Sirion), high resolution transmission electron microscopy (Tecnai 200KV), and Quantum design SQUID magnetometer (0–7 T, 5–300 K). A solution containing Fe_3O_4 nanowires in ethanol is dropped onto to a 500 nm SiO_2/Si substrate wafer and allowed it to dry under inert atmosphere. Fe_3O_4 nanowire (120 nm thickness) device with 3 μm channel length was fabricated using electron beam lithography and a 5 nm/100 nm thick Ti/Au electrodes were deposited using electron beam deposition.

X-ray diffraction data collected on as synthesized nanowire powder confirmed cubic magnetite (Fe_3O_4) phase purity matching the JCPDS index card 79–0416 (not shown here). A small degree of a polymer residue and a second cubic magnetite phase is observed in XRD spectra. Electron microscopy analyses were performed to understand morphology, microstructure, and crystalline phase of the nanowires. Scanning electron microscopy image, Figure 1(a), shows representative Fe_3O_4 nanowires with 80–120 nm thickness and lengths up to 8 μm with uniform morphology. A small percentage of Fe_3O_4 discs and polymer remainder were also observed along with the nanowires. Selected area electron diffraction (SAED) pattern showed the discs to be of cubic

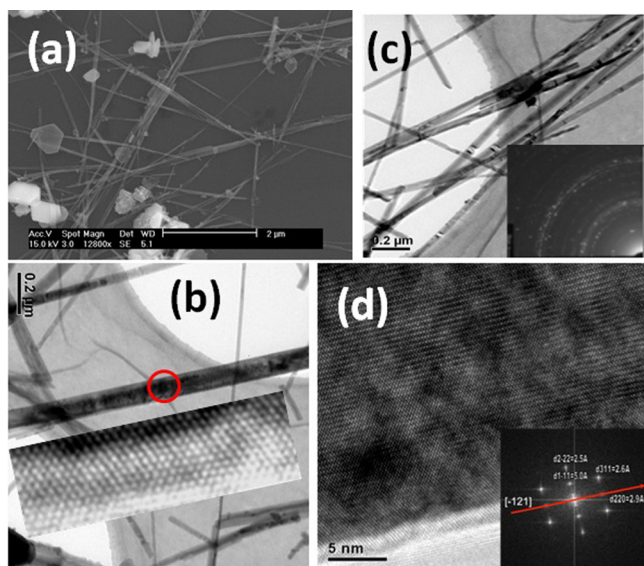


FIG. 1. Electron microscopy images showing Fe_3O_4 nanowires. (a) SEM image of Fe_3O_4 nanowires and discs morphology, (b) TEM images showing clean Fe_3O_4 nanowires, (inset) SAED pattern corresponding to Fe_3O_4 , (c) TEM image of single nanowire, (inset) high resolution image without any defects, collected from the red circle region, (d) high resolution micrograph showing clean Fe_3O_4 without any surface reconstruction or impurities, (inset) FFT image showing zone axis $[-121]$.

Fe_3O_4 phase (JCPDS index card 88-0866). High resolution transmission electron microscopy images in Figures 1(b) and 1(c) reveal morphology and highly crystalline microstructure of as prepared nanowires. SAED pattern inset, Figure 1(c), collected on few nanowires can be indexed to the cubic magnetite phase. It can be seen that SAED pattern of nanowires conforms well to that of XRD pattern. HRTEM image in Figure 1(d) collected from 80 nm wide single nanowire shows single crystalline nature of nanowire and possibly shows growth defects that can be related to antiphase boundaries. It can be realized that the core and surface of nanowire are well preserved and a Fast Fourier Transform (FFT) analysis shown in Figure 1(d) inset reveals the diffraction planes for single crystal magnetite nanowire. The analyzed zone axis for electron diffraction pattern for nanowire is $[-121]$ and the diffraction spots were indexed to (220), (311), and (111) lattice planes of Fe_3O_4 . Electron microscopy results show a very low percentage of defects and clearly establish the single crystallinity of the Fe_3O_4 nanowires.

Magnetic properties of single crystal Fe_3O_4 nanowires were evaluated using a SQUID magnetometer. Room temperature magnetic hysteresis was collected on nanowire powder sample without any preferred orientation of magnetic field. A saturation magnetization (M_s) of about 45 emu/g, 100 Oe coercivity, and a remanence magnetization (M_r) of 6.2 emu/g were observed for randomly oriented single crystal nanowire samples, as shown in Figure 2(a) indicating room temperature ferromagnetism. Figure 2(a) inset shows clear coercivity and remanent magnetization confirming ferromagnetism. The observed saturation magnetization is comparable to that of bulk and higher than other Fe_3O_4 nanocrystalline samples.¹⁹ Orientation of nanocrystallites, crystallinity, shape anisotropy, defects, and magnetostatic coupling are the key factors influencing saturation magnetization and other magnetic properties.^{20,21} Magnetic susceptibility measurements were carried out on the Fe_3O_4 nanowires to study possible phase transitions associated with temperature (5–300 K) and magnetic field dependence. Figure 2(b) shows zero-field cooled (ZFC) and field cooled (FC) magnetization for Fe_3O_4 nanowires with a 100 Oe applied magnetic field. With increasing temperature, the magnetization reaches a maximum value around 120 K for ZFC/FC measurements, which is defined as blocking temperature T_B in bulk Fe_3O_4 , where the thermal energy becomes comparable to the anisotropy energy barrier. Below T_B , magnetization of the nanowires aligns with the easy axis and anisotropy energy barriers would minimize magnetic moment with decreasing temperature. Above T_B , thermal energy overcomes the anisotropy and magnetic moments are aligned in the direction of external field. Blocking temperature is widely dependent on the magnetic interactions, morphology, and external agents.²² Above T_B , such "superparamagnetic" particles are expected to display zero coercivity and the FC and ZFC magnetizations will become identical. The clearly open hysteresis loops observed in our samples at $T > T_B$ (see data at 300 K shown in Fig. 2) and the continued divergence of FC and ZFC magnetizations for $T > T_B$ region suggest that 120 K is not a blocking temperature. The observed

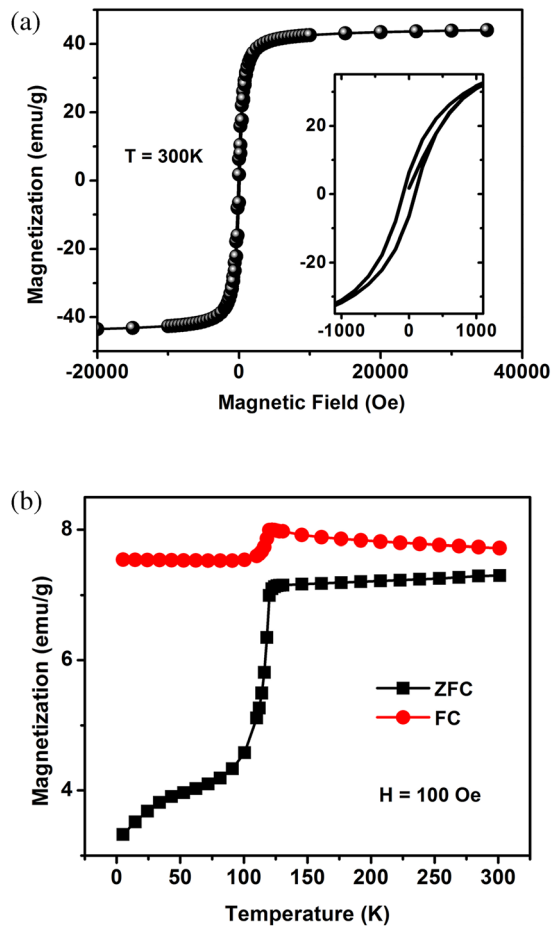


FIG. 2. Magnetization measurements collected on a bunch of Fe_3O_4 nanowires. (a) Room temperature hysteresis showing a $45 \text{ emu/g } M_s$, $6.2 \text{ emu/g } M_r$, and $\sim 100 \text{ Oe}$ coercivity. (Inset) An expanded hysteresis view to show the low field region, displaying coercivity. (b) Zero-field cooled and field cooled magnetization studies in $5 \text{ K} - 300 \text{ K}$ regime at a 100 Oe applied field. Verwey transition can be visualized around 120 K .

magnetization change at 120 K can be explained with Verwey transition.^{23,24} According to Verwey transition, Fe_3O_4 undergoes a charge ordering and structural ordering in the crystal lattice with crystallographic phase changing from cubic inverse spinel to monoclinic and the electrical properties display a metal-insulator transition as the temperature drops below 120 K . Verwey transition has profound effect on electrical properties of the Fe_3O_4 , which is discussed in the later section.

Figure 3 inset shows SEM image of Fe_3O_4 nanowire device fabricated using e-beam lithography. Electrical measurements performed in ambient conditions on the nanowire yielded a typical linear I-V curve showing Ohmic behavior for device. Figure 3 shows resistance from a single nanowire as a function of temperature in the $5 - 300 \text{ K}$ regime at a constant voltage bias. The circles represent resistance (R) data points acquired from original I-V scans and the line represents best fit. Electrical resistance of single Fe_3O_4 nanowire at room temperature is around $5 \times 10^{-4} \Omega \text{ m}$, which is comparable to epitaxial thin films^{14,25} and higher than bulk single crystal Fe_3O_4 .²⁶ Electrical resistance below 120 K is almost 2 orders of magnitude higher compared to room temperature. Above 120 K , the resistance decreased, which is in accordance with

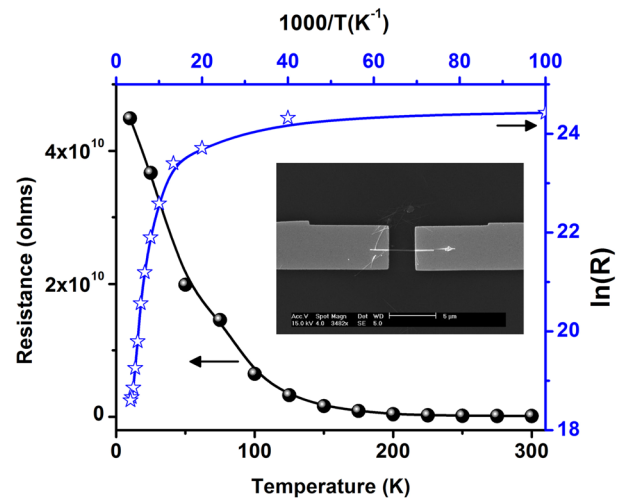


FIG. 3. Electrical resistance (left) measurements on a single Fe_3O_4 nanowire with temperature variation recorded at a constant voltage bias. Below 120 K (Verwey transition), the resistivity increased by 2 order of magnitude, while above 120 K a conducting behavior is observed. (Right) $\ln(R)$ vs $1000/T$ plot showing the activation energy around 0.07 eV . Inset shows a representative 120 nm thick Fe_3O_4 nanowire device with $3 \mu\text{m}$ channel length.

the Verwey transition. Above 120 K , Arrhenius plot shows linear relation, signifying thermally activated carrier transport mechanism at higher temperature. Activation energy ($\ln R$ vs $1000/T$) deduced from Figure 3 is around 0.07 eV . This value is in close agreement with similar morphology Fe_3O_4 nanowire/nanotube studies as well as bulk Fe_3O_4 .^{12,14,27}

Figure 4 shows 300 K MR measurements on a single crystal Fe_3O_4 nanowire device. Magnetic field is swept parallel to the nanowire from 0 to 0.3 T , keeping a constant voltage bias at a selected temperature. MR is calculated using equation, $\text{MR} = [R(H) - R(0)]/R(0)$, where $R(0)$ and $R(H)$ are resistance at zero field and at an applied field H , respectively. A total of 3 devices were tested and the value varied from -0.2% to -0.7% at a 0.3 T applied field. MR of Fe_3O_4 nanowires increased with applied magnetic field and did not show any saturation. A linear background is subtracted from measurement, as the actual MR signal was small. MR studies

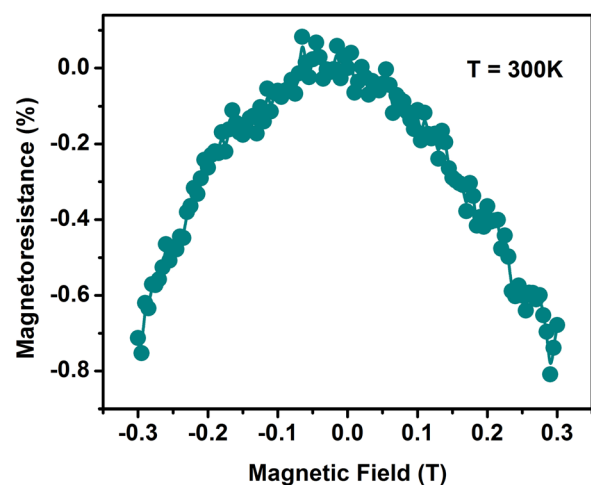


FIG. 4. Room temperature magnetoresistance plot showing a -0.7% MR at 0.3 T magnetic field collected from the single crystal Fe_3O_4 nanowire.

in single crystal Fe₃O₄ are quite inconsistent compared to that of bulk. Liao *et al.*¹⁶ reported anomalous positive MR $\sim 7.5\%$ in single crystal Fe₃O₄ nanowire, while Coey *et al.*² did not see any measurable MR in a single crystal Fe₃O₄. On the contrary, a negative MR is observed in this work. MR in the polycrystalline Fe₃O₄ is credited to magnetization in ferromagnetic grains, which are exchange-decoupled, or antiphase domains.² Considering the fact that the single crystal Fe₃O₄ nanowire is 120 nm thick there is a strong possibility for huge density of antiphase domain walls to be present. HRTEM (Figure 1(d)) possibly shows the antiphase domains present in the nanowire. The resulting magnetic coupling between antiphase boundaries is antiferromagnetic.^{28–30} When an external magnetic field is applied, neighboring antiphase boundary magnetic moment aligns in the direction of the field, resulting in reduced resistance. The absence of resistance saturation in Fe₃O₄ nanowire indicates the strong antiferromagnetic coupling of antiphase boundaries. Spin-polarized transport across antiphase boundaries in single crystal is analogous to epitaxial films, resulting in MR.

In summary, we demonstrated single crystal Fe₃O₄ nanowire showing a small but definite negative magnetoresistance at room temperature and attributed to the spin-polarized current resulting from antiphase domains. Nanowires were synthesized by a hydrothermal method and high resolution electron microscopy revealed cubic single crystalline magnetite. Room temperature electrical measurements have shown a resistance of $\sim 5 \times 10^{-4} \Omega \text{ m}$ on single nanowire and activation energy of 0.07 eV. Magnetic saturation and coercivity of Fe₃O₄ were found to be 45 emu/g and 100 Oe, respectively, at 300 K consistent with reported values for bulk Fe₃O₄. Inconsistent magnetoresistance properties from Fe₃O₄ single crystal nanowire are still debatable and needs further research attention. Our work demonstrates the experimental evidence of negative MR in Fe₃O₄ single crystal nanowires suggesting that spin based device integration can be realized.

¹M. Bibes and A. Barthelemy, "Oxide spintronics," *IEEE Trans. Electron Devices* **54**(5), 1003–1023 (2007).

²J. M. D. Coey *et al.*, "Magnetoresistance of magnetite," *Appl. Phys. Lett.* **72**(6), 734–736 (1998).

³J. M. D. Coey and C. L. Chien, "Half-metallic ferromagnetic oxides," *MRS Bull.* **28**(10), 720–724 (2003).

⁴Z. M. Liao *et al.*, "Magnetoresistance of Fe₃O₄-graphene-Fe₃O₄ junctions," *Appl. Phys. Lett.* **98**(5), 052511 (2011).

⁵G. Hu and Y. Suzuki, "Negative spin polarization of Fe₃O₄ in magnetite/manganite-based junctions," *Phys. Rev. Lett.* **89**(27), 276601 (2002).

⁶Y. S. Dedkov, U. Rudiger, and G. Guntherodt, "Evidence for the half-metallic ferromagnetic state of Fe₃O₄ by spin-resolved photoelectron spectroscopy," *Phys. Rev. B* **65**(6), 064417 (2002).

⁷J. M. De Teresa *et al.*, "Role of metal-oxide interface in determining the spin polarization of magnetic tunnel junctions," *Science* **286**(5439), 507–509 (1999).

⁸W. D. Wang, L. Malkinski, and J. K. Tang, "Enhanced spin-dependent tunneling magnetoresistance in magnetite films coated by polystyrene," *J. Appl. Phys.* **101**(9), 09J504 (2007).

⁹D. L. Peng *et al.*, "Magnetic properties and magnetoresistance in small iron oxide cluster assemblies," *Appl. Phys. Lett.* **81**(24), 4598–4600 (2002).

¹⁰W. Eerenstein *et al.*, "Spin-polarized transport across sharp antiferromagnetic boundaries," *Phys. Rev. Lett.* **88**(24), 247204 (2002).

¹¹R. V. Chopdekar *et al.*, "Magnetics and magnetoresistance in epitaxial magnetite heterostructures," *J. Electron. Mater.* **33**(11), 1254–1258 (2004).

¹²Z. Q. Liu *et al.*, "Single crystalline magnetite nanotubes," *J. Am. Chem. Soc.* **127**(1), 6–7 (2005).

¹³M. T. Chang *et al.*, "Magnetic and electrical characterizations of half-metallic Fe₃O₄ nanowires," *Adv. Mater.* **19**(17), 2290 (2007).

¹⁴D. H. Zhang *et al.*, "Magnetite (Fe₃O₄) core-shell nanowires: Synthesis and magnetoresistance," *Nano Lett.* **4**(11), 2151–2155 (2004).

¹⁵C. Terrier *et al.*, "Fe₃O₄ nanowires synthesized by electroprecipitation in templates," *J. Appl. Phys.* **98**(8), 086102 (2005).

¹⁶Z. M. Liao *et al.*, "Spin-filter effect in magnetite nanowire," *Nano Lett.* **6**(6), 1087–1091 (2006).

¹⁷L. T. Zhang *et al.*, "Positive and negative magnetoresistance in Fe₃O₄-based heterostructures," *J. Magn. Magn. Mater.* **324**(22), 3731–3736 (2012).

¹⁸K. Liu *et al.*, "Extrinsic magnetoresistance in magnetite nanoparticles," *J. Appl. Phys.* **93**(10), 7951–7953 (2003).

¹⁹S. H. Gee *et al.*, "Synthesis and aging effect of spherical magnetite (Fe₃O₄) nanoparticles for biosensor applications," *J. Appl. Phys.* **93**(10), 7560–7562 (2003).

²⁰T. G. Sorop *et al.*, "Study of the magnetic hysteresis in arrays of ferromagnetic Fe nanowires as a function of the template filling fraction," *J. Magn. Magn. Mater.* **272**, 1656–1657 (2004).

²¹S. Aravamudan *et al.*, "Magnetic properties of Ni-Fe nanowire arrays: Effect of template material and deposition conditions," *J. Phys. D: Appl. Phys.* **42**(11), 115008 (2009).

²²C. R. Vestal, Q. Song, and Z. J. Zhang, "Effects of interparticle interactions upon the magnetic properties of CoFe₂O₄ and MnFe₂O₄ nanocrystals," *J. Phys. Chem. B* **108**(47), 18222–18227 (2004).

²³E. J. W. Verwey, "Electronic conduction of magnetite (Fe₃O₄) and its transition point at low temperatures," *Nature* **144**, 327–328 (1939).

²⁴R. Prozorov *et al.*, "Magnetic irreversibility and the Verwey transition in nanocrystalline bacterial magnetite," *Phys. Rev. B* **76**(5), 054406 (2007).

²⁵S. P. Sena *et al.*, "Investigation of magnetite thin films produced by pulsed laser deposition," *J. Magn. Magn. Mater.* **176**(2–3), 111–126 (1997).

²⁶R. Prakash *et al.*, "Electrical and magnetic transport properties of Fe₃O₄ thin films on a GaAs(100) substrate," *J. Phys.: Condens. Matter* **19**(48), 486212 (2007).

²⁷A. Kozłowski *et al.*, "Electrical-conduction in single-crystal Fe₃-Yt_{1-y}O₄ (0 less-than Y less-than 0.9)," *Phys. Rev. B* **48**(4), 2057–2062 (1993).

²⁸W. Eerenstein *et al.*, "Magneto-resistance and superparamagnetism in magnetite films on MgO and MgAl₂O₄," *J. Magn. Magn. Mater.* **258**, 73–76 (2003).

²⁹W. Eerenstein *et al.*, "Diffusive motion of antiphase domain boundaries in Fe₃O₄ films," *Phys. Rev. B* **68**(1), 014428 (2003).

³⁰S. Celotto, W. Eerenstein, and T. Hibma, "Characterization of anti-phase boundaries in epitaxial magnetite films," *Eur. Phys. J. B* **36**(2), 271–279 (2003).